Articles

Soft Chemical Synthesis of New Layered and Three-Dimensional Oxide Hydrates, $H_xV_xW_{1-x}O_3 \cdot yH_2O$, Related to $WO_3 \cdot 2H_2O$ and $WO_3 \cdot {}^1/_3H_2O$†

J. Gopalakrishnan,* N. S. P. Bhuvanesh, and A. R. Raju‡

Solid State and Structural Chemistry Unit, Indian Institute of Science, Bangalore-560012, India

Received June 7, 1993. Revised Manuscript Received January 13, 1994®

Two new vanadium–tungsten oxide hydrates of the formulas, $H_{0.125}V_{0.125}W_{0.875}O_3 \cdot 1.5H_2O$ (**I**) and $H_{0.33}V_{0.33}W_{0.67}O_3 \cdot {}^1/_3H_2O$ (**II**), have been synthesized by acid-leaching of $LiVWO_6$ with aqueous HNO_3/HCl. While phase **I** obtained by treatment of $LiVWO_6$ with dilute HNO_3/HCl possesses an orthorhombic structure (a = 7.77(3), b = 13.87(6), c = 7.44(3) Å) related to $WO_3 \cdot 2H_2O$, phase **II**, prepared by refluxing $LiVWO_6$ with concentrated HNO_3, is isostructural with $WO_3 \cdot {}^1/_3H_2O$. Dehydration of **II** around 330 °C yields a hexagonal phase (**III**, a = 7.25(4), c = 7.74(3) Å) isotypic with hexagonal WO_3. Both **I** and **III** exhibit redox and acid–base intercalation reactivity characteristic of layered and tunnel structures.

Introduction

WO_3 and MoO_3 are two of the well-known transition-metal oxides which formed the basis for several advances in solid-state chemistry.[1] Besides being the parent materials for the tungsten[1] and molybdenum[2] bronzes and crystallographic shear phases,[1] both the oxides are excellent host materials for insertion/intercalation of a variety of chemical species.[3] WO_3 crystallizes in a ReO_3-like structure consisting of corner-connected $WO_{6/2}$ octahedra. MoO_3, on the other hand, adopts a unique layered structure consisting of double-octahedral layers formed by edge- and corner-sharing of ($MoO_{2/2}O_{3/3}$) octahedra.[4] Interestingly, the hydrates of both the oxides, $MO_3 \cdot 2H_2O$ and $MO_3 \cdot H_2O$ (M = Mo, W), are isotypic consisting of infinite $[MO_{4/2}O(H_2O)]$ layers.[4,5] WO_3 is also known to exist in two other metastable modifications,[6] the hexagonal WO_3 and the pyrochlore-like WO_3. A metastable MoO_3, isostructural with ReO_3-like WO_3, has also been synthesized by soft-chemistry routes.[7]

We have been investigating the synthesis of tungsten and molybdenum oxides as well as substitution of group V elements (Nb, Ta) in these oxides.[8] Recently, Feist and Davies[9] described a soft-chemical synthesis of new hexagonal vanadium–molybdenum oxides by acid-leaching of $AVMoO_6$ (A = Li, Na) brannerites. This prompted us to investigate similar acid-leaching of $LiVWO_6$ brannerite. Our investigations have led to the synthesis of two new vanadium–tungsten oxide hydrates, $H_{0.125}V_{0.125}W_{0.875}O_3 \cdot 1.5H_2O$ (**I**) and $H_{0.33}V_{0.33}W_{0.67}O_3 \cdot {}^1/_3H_2O$ (**II**). While **I** possesses a layered, $WO_3 \cdot 2H_2O$-like structure, **II** is formed with the $WO_3 \cdot {}^1/_3H_2O$ structure. Dehydration of **II** gives rise to a hexagonal WO_3-like $H_{0.33}V_{0.33}W_{0.67}O_3$ (**III**). Both **I** and **III** are novel host materials intercalating/inserting a variety of chemical species through redox as well as Bronsted acid–base type reactions. We describe in this paper the synthesis, characterization and investigation of the reactivity of these new vanadium–tungsten oxides.

Experimental Section

$LiVWO_6$ was prepared[10] by reacting Li_2CO_3 and V_2O_5 first at 550 °C for 24 h to give $LiVO_3$, which was subsequently heated with WO_3 in the required proportion at 650 °C for 24 h. X-ray

† Contribution no. 1005 from the Solid State and Structural Chemistry Unit.

* To whom correspondence should be addressed.

‡ Materials Research Centre, Indian Institute of Science, Bangalore.

® Abstract published in *Advance ACS Abstracts,* February 15, 1994.

(1) (a) Rao, C. N. R.; Gopalakrishnan, J. *New Directions in Solid State Chemistry*; Cambridge University Press: Cambridge, 1986. (b) Wadsley, A. D. In *Nonstoichiometric Compounds*; Mandelcorn, L., Ed.; Academic Press, New York, 1964. (c) Magnéli, A. *Pure Appl. Chem.* **1978**, *50*, 1261. (d) Kihlborg, L. *Ark. Kem.* **1963**, *21*, 471. (e) Ekström, T.; Tilley, R. J. D. *Chem. Scr.* **1980**, *16*, 1. (f) Ozin, G. A.; Özkar, S.; Prokopowicz, R. A. *Acc. Chem. Res.* **1992**, *25*, 553.

(2) Schlenker, C., Ed. *Low-Dimensional Electronic Properties of Molybdenum Bronzes and Oxides*; Kluwer: Dordrecht, 1989.

(3) (a) Whittingham, M. S. *MRS Bull.* Sept. **1989**. (b) Johnson, J. W.; Jacobson, A. J.; Rich, S. M.; Brody, J. F. *J. Am. Chem. Soc.* **1981**, *103*, 5246. (c) Genin, C.; Driouiche, A.; Gerand, B.; Figlarz, M. *Solid State Ionics* **1992**, *53–56*, 315. (d) Nazar, L. F.; Liblong, S. W.; Yin, X. T. *J. Am. Chem. Soc.* **1991**, *113*, 5889. (e) Nazar, L. F.; Zhang, Z.; Zinkweg, D. *J. Am. Chem. Soc.* **1992**, *114*, 6239.

(4) Wells, A. F. *Structural Inorganic Chemistry*, 5th ed.; Clarendon Press, Oxford, 1986.

(5) (a) Freedman, M. L. *J. Am. Chem. Soc.* **1959**, *81*, 3834. (b) Freedman, M. L.; Leber, S. *J. Less-Common Met.* **1964**, *7*, 427. (c) Krebs, B. *Acta Crystallogr.* **1972**, *B28*, 2222. (d) Günther, J. R. *J. Solid State Chem.* **1972**, *5*, 354. (e) Boudjada, N.; Rodriguez-Carvajal, J.; Anne, M.; Figlarz, M. *J. Solid State Chem.* **1993**, *105*, 211.

(6) Figlarz, M. *Prog. Solid State Chem.* **1989**, *19*, 1.

(7) (a) Harb, F.; Gerand, B.; Nowogrocki, G.; Figlarz, M. *C. R. Acad. Sci. Paris Ser. II* **1986**, *303*, 349. (b) McCarron III, E. M. *J. Chem. Soc., Chem. Commun.* **1986**, 336.

(8) (a) Ganapathi, L.; Ramanan, A.; Gopalakrishnan, J.; Rao, C. N. R. *J. Chem. Soc., Chem. Commun.* **1986**, 62. (b) Bhat, V.; Gopalakrishnan, J. *J. Chem. Soc., Chem. Commun.* **1986**, 1644. (c) Bhat, V.; Gopalakrishnan, J. *J. Solid State Chem.* **1986**, *63*, 278. (d) Bhat, V.; Gopalakrishnan, J. *Solid State Ionics* **1988**, *26*, 25.

(9) Feist, T. P.; Davies, P. K. *Chem. Mater.* **1991**, *3*, 1011.

(10) Galy, J.; Meunier, G.; Senegas, J.; Hagenmuller, P. *J. Inorg. Nucl. Chem.* **1971**, *33*, 2403.

0897-4756/94/2806-0373$04.50/0

powder diffraction pattern of the product was identical with that of $LiVWO_6$ brannerite reported in the literature.[10] Soft-chemical acid-leaching of $LiVWO_6$ was investigated by treating 1-g portions of the solid sample with 50-mL aliquots of HNO_3 or HCl of different concentrations for varying durations both over water bath and under reflux condition. The solid products, washed and dried after leaching, were examined by X-ray powder diffraction and EDX analysis. The extent of leaching of lithium into the aqueous phase was checked by flame photometry in select cases.

Two different single-phase materials (**I** and **II**) were obtained by acid-leaching of $LiVWO_6$: **I** with dilute (0.25–1 M) HNO_3 and HCl and **II** with concentrated (16 M) HNO_3 under reflux. At intermediate concentrations of HNO_3, mixtures of **I** and **II** were formed. With concentrated HCl, vanadium in $LiVWO_6$ was reduced to V(IV), giving a green solution. Both **I** and **II** are hydrated solids with 1.5 and $^1/_3H_2O$, respectively. Careful dehydration of **II** by heating a 2-g sample slowly (0.5 °C/min) to 330 °C and holding the sample at this temperature for 12 h yielded the anhydrous phase **III**.

Intercalation/insertion of atomic and molecular species into **I** and **III** was carried out by the usual methods. Reductive insertion of Li, Na, K, and NH_4 was carried out by treating 0.5 g of the solid samples with 25 mL of 0.5 M aqueous alkali metal/ammonium iodide solution[11] at room temperature. The extent of insertion was determined by titrating the liberated iodine with sodium thiosulfate. Intercalation of various organic amines in **I** was investigated by refluxing the solid with a 10% amine solution in *n*-heptane for several days. Insertion of ammonia vapors in **III** was carried out by the method described in ref 12.

A scanning electron microscope (Leica Cambridge Stereoscan S-360) fitted with Link AN-10000 EDX analyzer together with ZAF-4/FLS program was used for quantitative elemental analysis. A JEOL JDX-8P X-ray powder diffractometer operating with Cu Kα radiation was used to record X-ray diffraction (XRD) patterns. Unit-cell parameters were derived by least-squares refinement of powder diffraction data. Electron diffraction patterns were recorded with a JEOL JEM 200-CX transmission electron microscope. Water of hydration of the parent hydrates (**I** and **II**) and amine contents of intercalates were determined from weight losses in thermogravimetric curves. Thermogravimetric curves were recorded using a Cahn TG-131 system (heating rates 1–5 °C/min) in a flowing nitrogen atmosphere. Infrared spectra of powdered samples dispersed in KBr disks were recorded with a Bruker IFS-113V FT-IR spectrometer. Magnetic susceptibilities of hydrogen-insertion compounds of **III** were determined using a Lewis coil force magnetometer (George Associates, USA, Model 2000) at 5 kOe between 25 and 300 K.

Results and Discussion

Leaching of $LiVWO_6$ in HNO_3 yields two distinct solid phases, **I** and **II**; **I** is obtained in dilute (≤1 M) HNO_3 and **II** in concentrated (16 M) HNO_3. Leaching with dilute HCl similar to that reported by Feist and Davies[9] also yields **I**. Phase **I** is also obtained by leaching in dilute HCl of preheated (at 600 °C) mixtures of $Li_2W_2O_7$ and $LiVO_3$ having V/W ratios of 0.6 and 1.66. Leaching of $LiVWO_6$ in concentrated HCl, however, results in the reduction of vanadium. EDX analyses (Figure 1) show that the vanadium:tungsten ratio in **I** is approximately 1:7, and while the ratio for **II** is 1:2. Mass loss in thermogravimetric experiments (Figure 2) reveals that both **I** and **II** are hydrated with approximately 1.5 and 0.33 water molecules, respectively. Combining the EDX analysis and thermogravimetric data, the compositions of **I** and **II** could be written as $H_{0.125}V_{0.125}W_{0.875}O_3 \cdot 1.5H_2O$ (**I**) and $H_{0.33}V_{0.33}W_{0.67}O_3 \cdot {}^1/_3H_2O$ (**II**). Since lithium is leached out completely by acid treatment, protons are

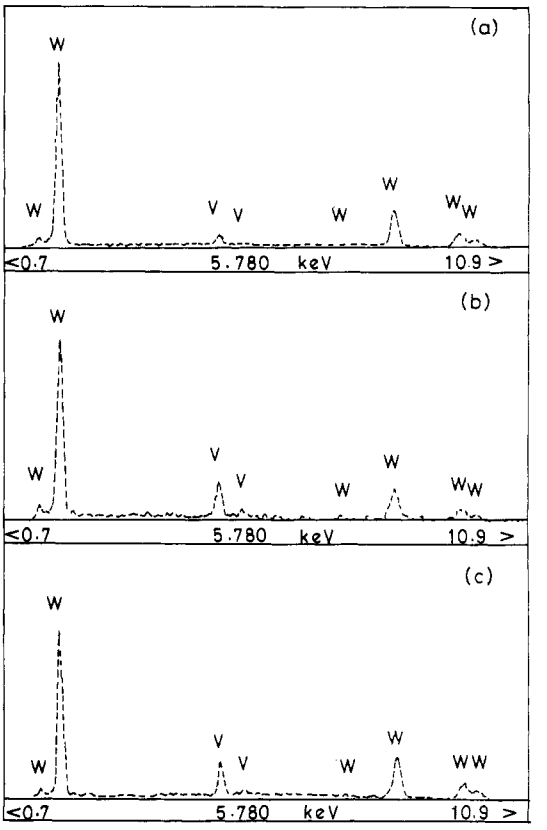

Figure 1. EDX spectra of (a) $H_{0.125}V_{0.125}W_{0.875}O_3 \cdot 1.5H_2O$ (**I**), (b) $H_{0.33}V_{0.33}W_{0.67}O_3 \cdot {}^1/_3H_2O$ (**II**), and (c) $H_{0.33}V_{0.33}W_{0.67}O_3$ (**III**).

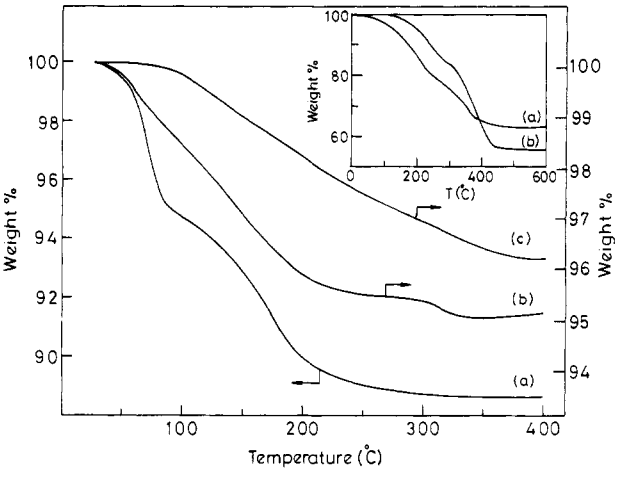

Figure 2. Thermogravimetric (TG) curves of (a) $H_{0.125}V_{0.125}W_{0.875}O_3 \cdot 1.5H_2O$ (**I**), (b) $H_{0.33}V_{0.33}W_{0.67}O_3 \cdot {}^1/_3H_2O$ (**II**), and (c) $(NH_4)_{0.30}H_{0.03}V_{0.33}W_{0.67}O_3$. In the inset are shown TG curves of intercalation compounds of **I** with (a) *n*-decylamine and (b) *n*-octadecylamine. TG curve (a) was recorded with a heating rate of 1 °C/min; for other curves the heating rate was 5 °C/min.

required for charge balance in **I** and **II**. The presence of protons in **I** and **II** is evidenced by the occurrence of an absorption band around 970–1000 cm^{-1} in the IR spectra (Figure 3). A similar band which has been attributed to V–O–H deformation is seen in the IR spectrum of $H_xV_2O_5$.[13]

Although the composition of **I** is closely similar to that of the hexagonal phase ($H_{0.13}V_{0.13}Mo_{0.87}O_3 \cdot nH_2O$) obtained by leaching the $LiVMoO_6$ in dilute HCl,[9] the XRD pattern

(11) Jacobson, A. J.; Johnson, J. W.; Brody, J. F.; Scanlon, J. C.; Lewandowski, J. T. *Inorg. Chem.* **1985**, *24*, 1782.
(12) Cao, G.; Mallouk, T. E. *Inorg. Chem.* **1991**, *30*, 1434.
(13) Dickens, P. G.; Chippindale, A. M.; Hibble, S. J.; Lancaster, P. *Mater. Res. Bull.* **1984**, *19*, 319.

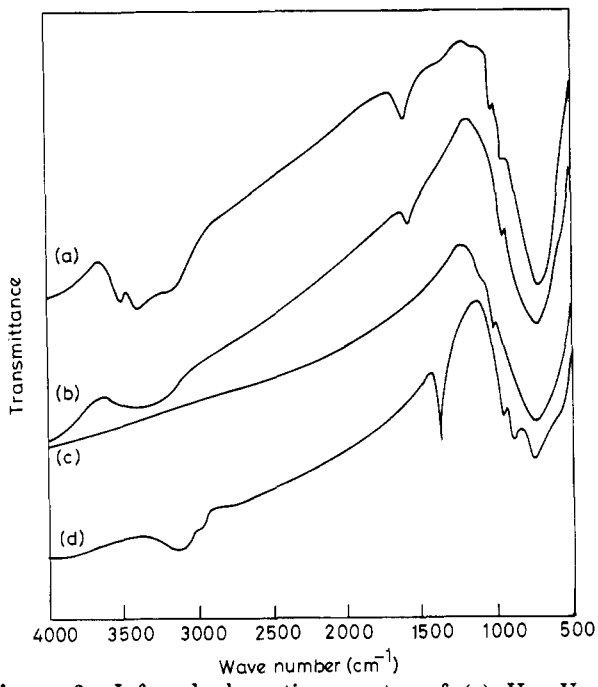

Figure 3. Infrared absorption spectra of (a) $H_{0.125}V_{0.125}W_{0.875}O_3 \cdot 1.5H_2O$ (**I**), (b) $H_{0.33}V_{0.33}W_{0.67}O_3 \cdot {}^1/_3H_2O$ (**II**), (c) $H_{0.33}V_{0.33}W_{0.67}O_3$, (**III**) and (d) $(NH_4)_{0.30}H_{0.03}V_{0.33}W_{0.67}O_3$.

Table 1. X-ray Powder Diffraction Data for $H_{0.125}V_{0.125}W_{0.875}O_3 \cdot 1.5H_2O$ (I)[a]

h k l	d_{obs} (Å)	d_{cal} (Å)	I_{obs}
0 2 0	6.94	6.93	100
1 0 1	5.39	5.38	25
2 0 0	3.883	3.887	5
2 1 0	3.739	3.742	45
0 4 0	3.473	3.467	55
0 2 2	3.284	3.281	64
1 4 0	3.164	3.166	8
2 0 2	2.675	2.686	6
2 1 2	2.633	2.640	16
2 4 0	2.585	2.587	10
0 4 2	2.536	2.537	16
1 5 1	2.465	2.465	10
0 6 0	2.309	2.311	9
3 1 2	2.094	2.102	5
0 6 2	1.959	1.964	16
4 2 0	1.866	1.871	11
0 2 4	1.797	1.798	10
0 8 0	1.734	1.734	8
2 1 4	1.667	1.667	5
0 4 4	1.639	1.640	10
2 2 4	1.634	1.632	9
4 3 2	1.618	1.614	10
3 6 2	1.568	1.565	5

[a] a = 7.77(3), b = 13.87(6), c = 7.44(3) Å.

of **I** (Figure 4a) is distinctly different. The pattern is indexable on the orthorhombic cell with a = 7.77(3), b = 13.87(6), c = 7.44(3) Å (Table 1). Thermogravimetry of **I** (Figure 2a) shows the formation of an intermediate hydrate, $H_{0.125}V_{0.125}W_{0.875}O_3 \cdot 0.8H_2O$, whose XRD pattern (Figure 4b) is similar to that of $WO_3 \cdot H_2O$.[5b,14] We could index this pattern on an orthorhombic cell (a = 5.24(4), b = 10.61(7), c = 5.14(3) Å) similar to that of $WO_3 \cdot H_2O$.[5e] On complete dehydration, phase **I** transforms to a WO_3-like structure at ≥400 °C. Accordingly, we believe that the structure of phase **I** is closely related to that of $WO_3 \cdot 2H_2O/MoO_3 \cdot 2H_2O$.[5c] In an attempt to provide further support to the relationship between the structures of phase **I** and $WO_3 \cdot 2H_2O$, we prepared a sample of $WO_3 \cdot 2H_2O$ according to the method of Freedman.[5a] Indeed, we see that the XRD pattern of phase **I** (Figure 4a) bears a close relationship to the pattern of $WO_3 \cdot 2H_2O$ (Figure 4c). $WO_3 \cdot 2H_2O$ (and the isostructural $MoO_3 \cdot 2H_2O$) crystallize in a monoclinic layered structure[5c,e,15] with a_m = 10.53, b_m = 13.84, c_m = 10.53 Å, β_m = 90.08°. The orthorhombic cell of phase **I** is probably related to the monoclinic cell of $WO_3 \cdot 2H_2O/MoO_3 \cdot 2H_2O$ as follows:

$$\sqrt{2}a(\mathbf{I}) \simeq c_m$$

$$b(\mathbf{I}) \simeq b_m$$

$$\sqrt{2}c(\mathbf{I}) \simeq a_m$$

A significant difference between the two XRD patterns (Figure 4a,c) is the presence of a strong reflection at d = 5.39 Å in the pattern of phase **I**, which is absent in the pattern of $WO_3 \cdot 2H_2O$. This reflection, which is indexable as (101) of the orthorhombic cell (Table 1), accounts for the $\sqrt{2}$ relationship between the a and c axes of the orthorhombic and monoclinic cells. Intercalation of *n*-alkylamines resulting in large increases in the b parameter (see later) provides further support to the layered structure of phase **I** (Figure 5a). A determination of the actual structure by X-ray or neutron diffraction is essential to reveal the exact relationship between the structures of phase **I** and $WO_3 \cdot 2H_2O/MoO_3 \cdot 2H_2O$.

The XRD pattern of phase **II** (Figure 4d) closely resembles the pattern of $WO_3 \cdot {}^1/_3H_2O$ reported by Gerand et al.[16] We could index all the reflections in the diffraction pattern, by comparison with the pattern of $WO_3 \cdot {}^1/_3H_2O$, in an orthorhombic cell with a = 7.22(3), b = 12.54(7), c = 7.66(4) Å (Table 2). Accordingly, phase **II** could be regarded as a derivative of $WO_3 \cdot {}^1/_3H_2O$ wherein a third of W(VI) in the framework is replaced by V(V), the charge balance being achieved by the incorporation of protons leading to the formula $H_{0.33}V_{0.33}W_{0.67}O_3 \cdot {}^1/_3H_2O$. A calculation of the XRD intensities of phase **II** by the LAZY PULVERIX program using the position parameters of the $WO_3 \cdot {}^1/_3H_2O$ structure[16] and assuming that W sites are occupied by ${}^1/_3V + {}^2/_3W$ indeed gives a good agreement with the observed intensities (Table 2).

The structure of $WO_3 \cdot {}^1/_3H_2O$ (space group $Fmm2$)[16] consists of infinite sheets of WO_6 octahedra sharing corners to form six-membered rings as in the hexagonal tungsten bronze (HTB) structure.[17] The sheets are stacked one over the other along the [001] direction, the alternate sheets being shifted by $a/2$ (Figure 5b). In view of the close relationship between $WO_3 \cdot {}^1/_3H_2O$ and HTB, $WO_3 \cdot {}^1/_3H_2O$ topotactically dehydrates to give a new form of WO_3 (h-WO_3) that possesses the framework of the HTB structure wherein the hexagonal tunnels are empty (Figure 5c).[18] Since phase **II** prepared by us is isostructural with $WO_3 \cdot {}^1/_3H_2O$, we expected that **II** would dehydrate to give a new vanadium-tungsten oxide that is isostructural with h-WO_3. Accordingly, dehydration of phase **II** yields anhydrous $H_{0.33}V_{0.33}W_{0.67}O_3$ (phase **III**) whose XRD pattern closely resembles that of h-WO_3.[18] The pattern

(14) Szymanski, J. T.; Roberts, A. C. *Can. Mineral.* **1984**, *22*, 681.

(15) Mitchell, R. S. *Am. Miner.* **1963**, *48*, 935.

(16) Gerand, B.; Nowogrocki, G.; Figlarz, M. *J. Solid State Chem.* **1981**, *38*, 312.

(17) Magnéli, A. *Acta Chem. Scand.* **1953**, *7*, 315.

(18) Gerand, B.; Nowogrocki, G.; Guenot, J.; Figlarz, M. *J. Solid State Chem.* **1979**, *29*, 429.

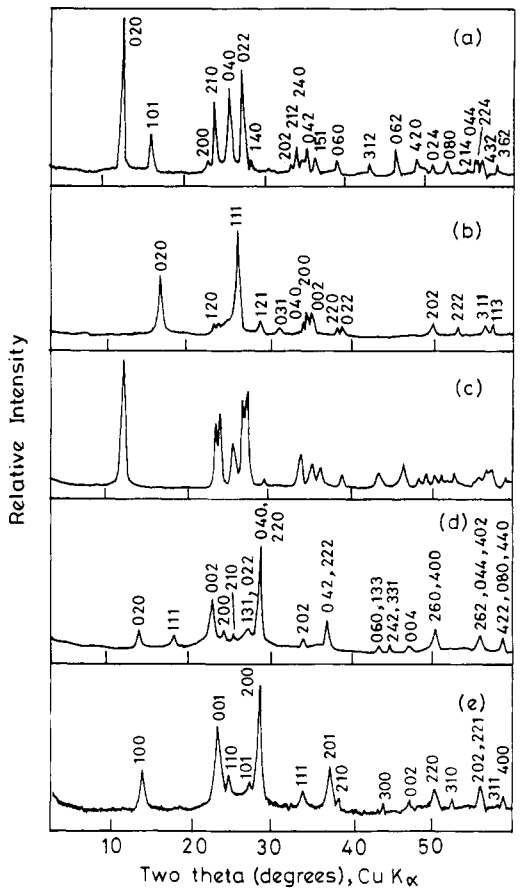

Figure 4. X-ray powder diffraction patterns of (a) $H_{0.125}V_{0.125}W_{0.875}O_3 \cdot 1.5H_2O$ (**I**), (b) $H_{0.125}V_{0.125}W_{0.875}O_3 \cdot 0.8H_2O$ obtained from I, (c) $WO_3 \cdot 2H_2O$, (d) $H_{0.33}V_{0.33}W_{0.67}O_3 \cdot {}^1/_3H_2O$ (**II**), and (e) $H_{0.33}V_{0.33}W_{0.67}O_3$ (**III**).

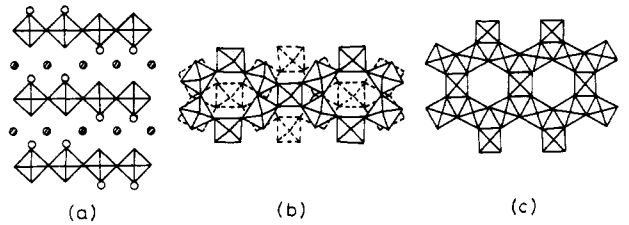

Figure 5. Schematic representation of the structures of (a) $H_{0.125}V_{0.125}W_{0.875}O_3 \cdot 1.5H_2O$ (**I**), (b) $H_{0.33}V_{0.33}W_{0.67}O_3 \cdot {}^1/_3H_2O$ (**II**), and (c) $H_{0.33}V_{0.33}W_{0.67}O_3$ (**III**).

of phase **III** (Figure 4e) is indexable on a hexagonal cell with a = 7.25(4), c = 3.87(2) Å (Table 3). Calculation of XRD intensities of this phase by LAZY PULVERIX program for the h-WO_3 structure assuming that the W sites are occupied by $^1/_3$V + $^2/_3$W gives a good agreement with the observed intensities of *hkl* reflections (Table 3). Electron diffraction patterns of this phase (Figure 6), while confirming the hexagonal structure, reveal the presence of a c-axis doubling, just as in the case of h-WO_3 structure.[18] Accordingly, the true cell parameters of III would be a = 7.25(4), c = 7.74(3) Å, and Z = 6. The slight decrease in the cell parameters of III as compared to those of h-WO_3 (a = 7.298(2), c = 7.798(3) Å) most likely reflects the replacement of larger W(VI) by the smaller V(V). Phase **III** is metastable, transforming to an oxygen-deficient WO_3-like $V_{0.33}W_{0.67}O_{3-y}$ ($y \sim 0.165$) on heating above 400 °C.

We expected that layered $WO_3 \cdot 2H_2O$-like phase **I** and hexagonal WO_3-like phase **III**, containing vanadium(V) and acidic protons, would exhibit interesting intercalation reactivity. Accordingly, we investigated both redox intercalation and acid–base intercalation in **I** and **III**. We could readily insert alkali metal (Li, Na, K) and ammonium ions in both **I** and **III** by treating the host solids with an aqueous solution of alkali metal/ammonium iodide, the insertion occurring according to the redox reaction

$$H_xV_xW_{1-x}O_3 \cdot yH_2O + zAI \rightarrow A_z[H_xV_xW_{1-x}O_3 \cdot yH_2O] + (z/2)I_2$$

The compositions of insertion compounds of **I** and **III**

Table 2. X-ray Powder Diffraction Data for $H_{0.33}V_{0.33}W_{0.67}O_3 \cdot {}^1/_3H_2O$ (II)[a]

h k l	d_{obs} (Å)	d_{cal} (Å)	I_{obs}	I_{cal}[b]
0 2 0	6.26	6.27	21	22
1 1 1	4.835	4.845	15	51
0 0 2	3.834	3.828	48	51
2 0 0	3.619	3.610	12	5
2 1 0	3.473	3.469	7	
1 3 1	3.261	3.271	22	16
0 2 2		3.270		16
0 4 0	3.132	3.135	100	100
2 2 0		3.130		
2 0 2	2.629	2.626	7	7
0 4 2	2.423	2.425	29	12
2 2 2		2.423		29
0 6 0	2.092	2.090	4	1
1 3 3		2.086		3
2 4 2	2.010	2.013	10	3
3 3 1		2.012		6
0 0 4	1.914	1.914	5	6
2 6 0	1.807	1.809	22	13
4 0 0		1.805		7
2 6 2	1.637	1.635	18	10
0 4 4		1.634		4
4 0 2		1.633		5
4 2 2	1.568	1.580	12	2
0 8 0		1.568		4
4 4 0		1.564		7

[a] a = 7.22(3), b = 12.54(7), c = 7.66(4) Å. [b] Calculated by LAZY PULVERIX program using the position parameters of $WO_3 \cdot {}^1/_3H_2O$ structure[16] assuming that W sites are occupied by $^1/_3$V + $^2/_3$W.

Table 3. X-ray Powder Diffraction Data for $H_{0.33}V_{0.33}W_{0.67}O_3$ (III)[a]

h k l	d_{obs} (Å)	d_{cal} (Å)	I_{obs}	I_{cal}[b]
1 0 0	6.27	6.28	60	80
0 0 1	3.867	3.872	71	70
1 1 0	3.633	3.627	30	23
1 0 1	3.290	3.296	23	23
2 0 0	3.143	3.141	100	100
1 1 1	2.652	2.647	10	12
2 0 1	2.436	2.439	43	54
2 1 0	2.371	2.375	5	4
3 0 0	2.094	2.094	5	8
0 0 2	1.929	1.936	12	16
2 2 0	1.819	1.814	25	29
3 1 0	1.748	1.742	8	7
2 0 2	1.642	1.648	26	31
2 2 1		1.642		
3 1 1	1.586	1.588	3	7
4 0 0	1.570	1.571	9	18

[a] a = 7.25(4), c = 3.87(2) Å. [b] Calculated by LAZY PULVERIX program using the position parameters of h-WO_3 structure[18] assuming that W sites are occupied by $^1/_3$V + $^2/_3$W.

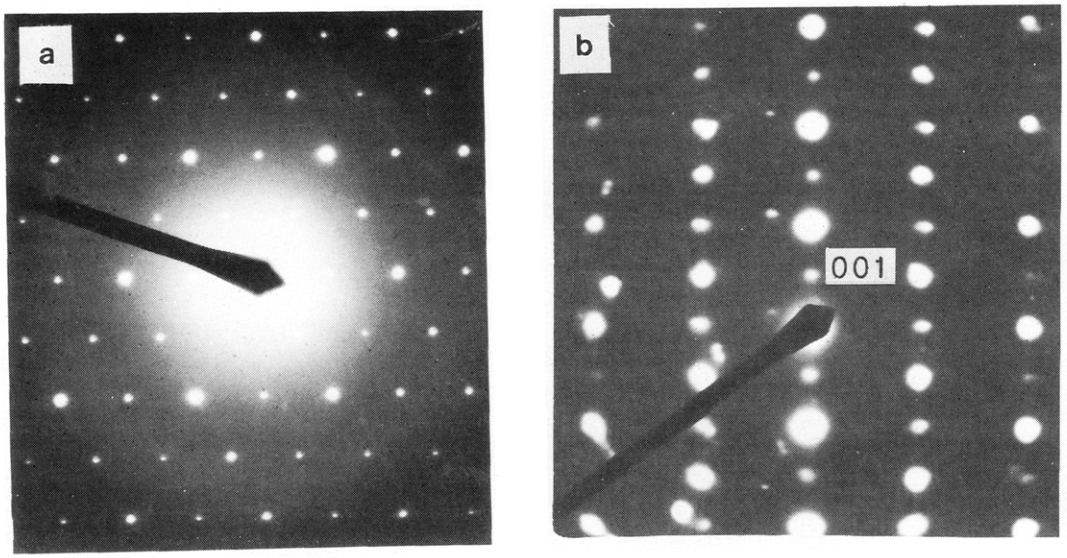

Figure 6. Electron diffraction patterns of $H_{0.33}V_{0.33}W_{0.67}O_3$ (**III**). (a) [001]* and (b) [100]* reciprocal sections.

Table 4. Composition, Color, and Lattice Parameters of $H_{0.125}V_{0.125}W_{0.875}O_3 \cdot 1.5H_2O$ (I) and Its Insertion Compounds

compound	color	reducing power[a]	lattice parameters (Å)		
			a	*b*	*c*
$H_{0.125}V_{0.125}W_{0.875}O_3 \cdot 1.5H_2O$	reddish brown		7.77(3)	13.87(6)	7.44(3)
$Na_{0.25}[H_{0.125}V_{0.125}W_{0.875}O_3 \cdot 1.5H_2O]$	dark green	0.25	7.62(4)	13.77(9)	7.41(5)
$K_{0.18}[H_{0.125}V_{0.125}W_{0.875}O_3 \cdot 1.5H_2O]$	dark green	0.18	7.63(3)	13.74(7)	7.41(3)
$(NH_4)_{0.26}[H_{0.125}V_{0.125}W_{0.875}O_3 \cdot 1.5H_2O]$	dark green	0.26	7.79(6)	13.82(7)	7.42(3)

[a] The reducing power, which corresponds to the lower oxidation state of V/W, is determined by titrating the liberated iodine.

Table 5. Composition, Color, and Lattice Parameters of $H_{0.33}V_{0.33}W_{0.67}O_3$ (III) and Its Insertion Compounds

compound	color	vanadium %		reducing power[a]	lattice parameters (Å)	
		found	calcd		*a*	*c*[b]
$H_{0.33}V_{0.33}W_{0.67}O_3$	reddish brown	8.90	8.93		7.25(4)	3.87(2)
$Li_{0.37}[H_{0.33}V_{0.33}W_{0.67}O_3]$	dark green	8.83	8.81	0.36	7.24(3)	3.86(2)
$Na_{0.33}[H_{0.33}V_{0.33}W_{0.67}O_3]$	dark green	8.67	8.58	0.33	7.25(3)	3.87(2)
$K_{0.33}[H_{0.33}V_{0.33}W_{0.67}O_3]$	dark green	8.38	8.34	0.34	7.25(4)	3.87(3)
$H_{0.90}[H_{0.33}V_{0.33}W_{0.67}O_3]$	bluish black	8.74	8.88	0.90	7.26(2)	3.87(2)
$H_{0.62}[H_{0.33}V_{0.33}W_{0.67}O_3]$	bluish black	8.94	8.90	0.62	7.26(3)	3.87(2)
$(NH_4)_{0.25}[H_{0.33}V_{0.33}W_{0.67}O_3]$	bluish black	8.71	8.76	0.25	7.26(2)	3.87(1)
$(NH_4)_{0.30}[H_{0.03}V_{0.33}W_{0.67}O_3]$	yellowish brown	8.62	8.69		7.24(2)	3.86(1)

[a] The reducing power, which corresponds to the lower oxidation state of V/W, is determined by titrating the liberated iodine (in the case of alkali-metal insertion compounds) or by redox potentiometric titration using Ce(IV) as oxidant. [b] For the true cell, *c* should be doubled.

together with their lattice parameters are listed in Tables 4 and 5. The XRD patterns of a few typical insertion compounds are given in Figures 7 and 8. We see that the extent of insertion (z) in all the insertion compounds of **III** is around 0.33, while the extent of insertion in **I** is in the range 0.18–0.25. It it likely that only vanadium is reduced to V(IV) in **III** by the insertion of alkali metal.

We could also insert hydrogen into **III** by passing hydrogen gas over the solid dispersed with 1 wt % Pt. Insertion readily occurs at room temperature giving $H_{0.90}[H_{0.33}V_{0.33}W_{0.67}O_3]$ that retains the parent HTB structure (Figure 8b). When the insertion is carried out at 200 °C, the composition of the insertion compound is $H_{0.62}[H_{0.33}V_{0.33}W_{0.67}O_3]$ (Table 5). It is possible that in the latter only V(V) is reduced to V(III), while in the former some of the W(VI) is also reduced. Magnetic susceptibility measurements show that the blue-black hydrogen-insertion compounds are Curie–Weiss paramagnetic. The magnetic moments per transition metal atom, obtained from the χ^{-1}_M–T plots (Figure 9), are 0.80 and 1.20 μ_B, respectively for the $H_{0.62}$ and $H_{0.90}$ phases. The room-temperature electrical resistivities are around 10^5–10^6 Ω cm, indicating that the phases are semiconducting.

Besides the redox intercalation reactivity, both **I** and **III** exhibit acid–base intercalation due to the Bronsted acidity of the protons present in the interlayer region/tunnels of the host structure. **I** readily forms intercalation compounds with a number of *n*-alkylamines. In Table 6 we list the composition and lattice parameters of the amine intercalates of **I**. In Figure 2 (inset) we give the TG curves of typical amine intercalates, and in Figure 7 we show the X-ray powder diffraction patterns of representative amine intercalates. Two features are noteworthy. We see that the amine intercalation results in large layer expansions characteristic of intercalation of *n*-alkylamines in layered structures.[19] A lattice expansion of ≥2.05 Å/carbon is indicative of a bilayer configuration of the intercalated amine in all the cases.[12,19] A plot of the interlayer distance vs the number of carbon atoms in the *n*-alkylamines (Figure 10) shows that the data points for C_6–C_{12} amines fall on a straight line that fits to the equation $b/2 = 2.06n + 7.87$ Å. Accordingly, we infer that the alkyl chains are oriented

(19) (a) Whittingham, M. S., Jacobson, A. J., Eds. *Intercalation Chemistry*; Academic Press, New York, 1982. (b) Beneke, K.; Lagaly, G. *Inorg. Chem.* **1983**, *22*, 1503. (c) Jacobson, A. J.; Johnson, J. W.; Lewandowski, J. T. *Mater. Res. Bull.* **1987**, *22*, 45.

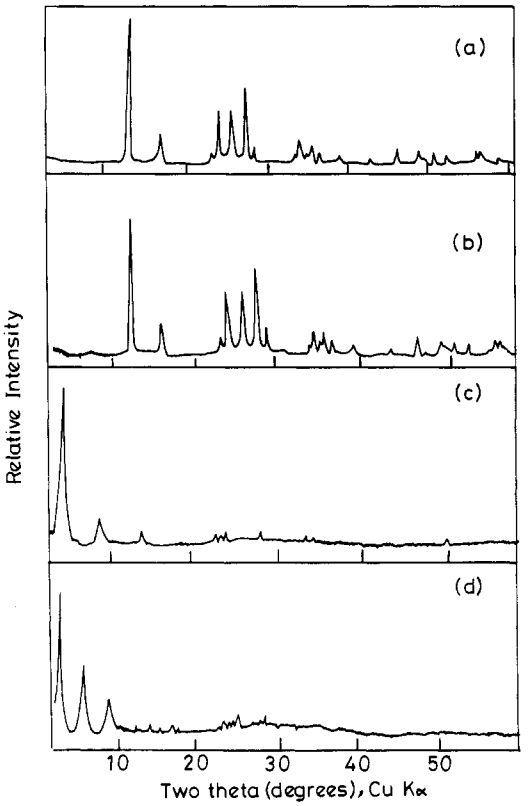

Figure 7. X-ray powder diffraction patterns of insertion compounds of **I** with (a) Na, (b) NH_4, (c) *n*-hexylamine, and (d) *n*-decylamine.

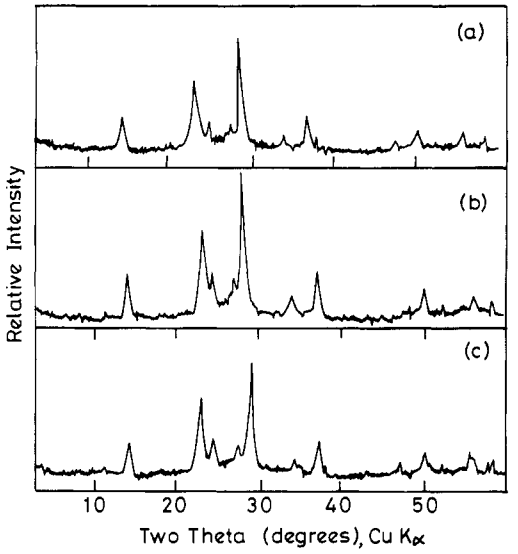

Figure 8. X-ray powder diffraction patterns of insertion compounds of **III** with (a) Na, (b) H, and (c) NH_3.

at an angle of $\sin^{-1}(2.06/(2 \times 1.27)) = 54°$. Significantly, the layer expansions of the C_{16} and C_{18} amine intercalates do not fit this equation, indicating a different orientation of the alkyl chain. Another noteworthy feature is that the quantity of the amine intercalated is more than the proton content of the host, suggesting that neutral amine molecules are also present along with *n*-alkylammonium ions in the interlamellar region. A similar behavior has been reported with other layered hosts.[20]

(20) (a) Lagaly, G.; Beneke, K.; Weiss, A. *Am. Mineral.* **1975**, *60*, 642. (b) Kinomura, N.; Onda, K.; Kobayashi, M.; Kumada, N.; Muto, F. *J. Mater. Sci.* **1989**, *24*, 1814.

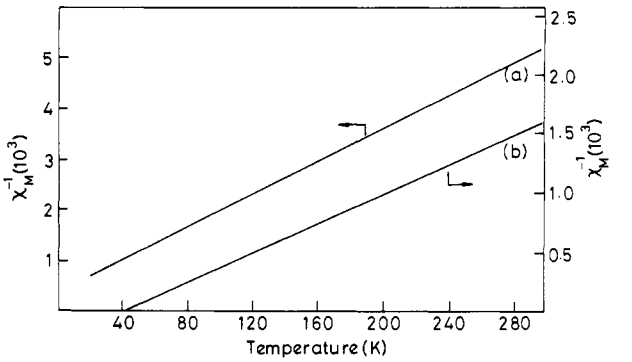

Figure 9. Plots of inverse molar susceptibilities, χ^{-1}_M, versus temperature, *T*, for (a) $H_{0.62}[H_{0.33}V_{0.33}W_{0.67}O_3]$ and (b) $H_{0.90}[H_{0.33}V_{0.33}W_{0.67}O_3]$.

Table 6. Composition and Lattice Parameters of Amine Intercalation Compounds of $H_{0.125}V_{0.125}W_{0.875}O_3 \cdot 1.5H_2O$ (I)

intercalate	lattice parameters (Å) *a*	*b*	*c*	intercalated amine content[a]	$\Delta d/n$[b] (Å)
n-hexylamine	7.69(3)	39.0(2)	7.44(3)	0.57	2.09
n-heptylamine	7.93(5)	45.4(2)	7.33(4)	0.58	2.25
n-octylamine	7.73(2)	49.0(1)	7.28(1)	0.63	2.20
n-nonylamine	7.65(8)	52.6(6)	7.20(8)	0.73	2.15
n-decylamine	7.78(9)	58.0(6)	7.55(9)	0.61	2.21
n-dodecylamine	7.93(5)	64.0(8)	7.39(4)	0.60	2.09
n-hexadecylamine	7.67(5)	89.8(9)	7.29(7)	0.41	2.37
n-octadecylamine	7.89(6)	105.1(6)	7.39(5)	0.61	2.53

[a] Denotes number of formula units of amine intercalated per formula unit of **I**. [b] Denotes interlayer expansion per carbon due to intercalation. *d* is *b*/2.

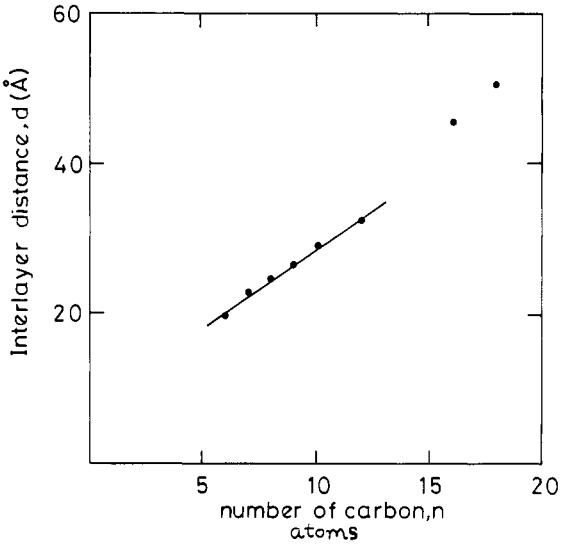

Figure 10. Plot of interlayer distance vs. number of carbon atoms in the *n*-alkylamine intercalates of **I**.

Finally, ammonia insertion in **III** deserves a special mention. Phase **III** readily absorbs vapors of ammonia at room temperature. The composition (Figure 2 and Table 5) and IR spectrum (Figure 3) of the ammonia insertion compound reveal that the NH_3 inserted is protonated to NH_4^+. We see characteristic absorption bands[21] of NH_4^+ at 3190 and 1410 cm^{-1} in the spectrum. Ammonia insertion in **III** does not however result in a significant change in the lattice parameters of the host, probably because the ammonia molecules occupy the hexagonal tunnels of this structure, without changing the

(21) Nakamoto, K. *Infrared Spectra of Inorganic and Coordination Compounds*, 3rd ed.; Wiley: New York, 1978; p 135.

dimensions of the framework. The insertion of NH_3, which is a special property of **III** and not exhibited by h-WO_3, is presumably due to the acidic protons present in the host.

Conclusion

In this paper, we have described the synthesis of two new vanadium–tungsten oxide hydrates, $H_{0.125}V_{0.125}W_{0.875}O_3 \cdot 1.5H_2O$ (**I**) and $H_{0.33}V_{0.33}W_{0.67}O_3 \cdot {}^1/_3H_2O$ (**II**), by a soft-chemical method involving acid-leaching of $LiVWO_6$. While **I** adopts a $WO_3 \cdot 2H_2O$-like layered structure, **II** is isostructural with $WO_3 \cdot {}^1/_3H_2O$. **II** dehydrates around 330 °C to give a new hexagonal-WO_3-like derivative, $H_{0.33}V_{0.33}W_{0.67}O_3$ (**III**). Both **I** and **III** are novel host materials exhibiting redox and acid–base intercalation reactivity, the latter arising from the acidic protons present in the host materials.

Acknowledgment. We thank Professor C. N. R. Rao for valuable support and encouragement. Our special thanks are due to Professor P. K. Davies and Professor M. Figlarz for valuable discussions on the structure and reactivity of the new phases reported in this paper. We also thank Dr. G. N. Subbanna for recording the electron diffraction patterns and the Department of Science and Technology, Government of India, for financial support.